INTERNATIONAL JOURNAL FOR NUMERICAL METHODS IN FLUIDS
Int. J. Numer. Meth. Fluids 2000; **32**: 669–690

Analysis of high speed non-equilibrium chemically reacting gas flows. Part I. Physical modeling and sensitivity studies

Christophe Harlé, Graham F. Carey* and Philip L. Varghese

CFD Laboratory, ASE/EM Department, WRW 301, The University of Texas at Austin, Austin, TX 78712, U.S.A.

SUMMARY

In this part, a theoretical model for high speed flow of chemically reacting gases out of thermal and chemical equilibrium is presented. The main features of the physical model are discussed together with details for a new form of the kinetic rate coefficients for non-equilibrium flows and presentation of a two-layer radiation model used for a plasma torch problem. This model is implemented in a new hybrid finite volume/finite element scheme, which is developed in Part II. Results from this physical model are compared with experiments and other results in the literature for an arcjet and non-equilibrium nozzle test case. Sensitivity studies are included for the nozzle problem to simulate the influence of the rate coefficients. Copyright © 2000 John Wiley & Sons, Ltd.

KEY WORDS: non-equilibrium flow; reacting gas flow; sensitivity study

1. INTRODUCTION

There has been a resurgence of interest in computing hypersonic flows for reentry vehicles and the National Aerospace plane in the U.S., or the Hermes space shuttle in Europe. This subject is also important for designing ground testing facilities, such as high enthalpy wind tunnels or plasma torches [1,2], and has led to two main areas of research: the physical modeling of chemically reacting real gases in high speed flows, and the construction of mathematical models and numerical schemes to perform calculations of high enthalpy flow. Of particular interest are calculations of viscous reacting gases out of thermal and chemical equilibrium [3–5].

The difficulty associated with these flow problems stems from two primary sources. First, the phenomenological models used to describe the molecular mechanisms that drive a gas to thermal and chemical equilibrium have been validated at modest temperatures (up to 5000 K

* Correspondence to: CFD Laboratory, ASE/EM Department, WRW 301, The University of Texas at Austin, Austin, TX 78712, U.S.A.

Received 11 August 1995
Revised 1 June 1999

typically), and weak thermal non-equilibrium. There is considerable uncertainty in the model predictions when they are extrapolated to higher temperatures, where thermal and chemical non-equilibrium occur simultaneously. Second, the fluid dynamic equations describing the flow field are more complicated than standard viscous compressible flows at moderate speeds, where chemistry and radiation are not important. Hence, there is considerable interest in developing schemes that can handle non-equilibrium flows. The purpose of this paper (Part I) is to develop a multi-temperature theoretical model for chemically reacting gases out of thermal and chemical equilibrium, including radiation effects. Part II will present details of the conservative hybrid finite element/finite volume scheme that has been used in these simulation studies.

The physical model developed in this work is an extension of the models described in References [6,7]. At present, very few experimental results are available for high enthalpy flow. However, certain benchmark problems have been defined to guide the applications and design studies via numerical simulation of this demanding class of flow problem [2]. In the present work, numerical results for relevant external and internal flow problems are compared with numerical simulations available in the literature in order to benchmark the computational scheme. Results are also compared with available experimental data.

The outline of this part is as follows: in the first section, a system of equations is formulated to describe a continuum reacting viscous flow out of thermal and chemical equilibrium. The main physical model is presented and details of models of non-equilibrium kinetic rate coefficients for the chemical reactions are given. In particular, a theoretical correction for the kinetic rate coefficients of non-equilibrium flows is described in Section 2.4. A new simple radiative model is introduced in Section 3, as a first approximation for optically thick or transparent gas calculations. Finally, results for non-equilibrium flow in a converging–diverging nozzle are compared with results in the literature, and sensitivity studies for the rate coefficients are performed.

2. PHYSICAL MODEL

2.1. Thermal and chemical non-equilibrium

Here, a multi-species gas out of thermal and chemical equilibrium is considered. At a macroscopic level, the interaction between species is described by a set of chemical reactions (dissociation/recombination reactions, exchange reactions, ionization reactions). These interactions and radiative excitation contribute to modify the internal modes of each species. For atoms, the translational and the electronic internal modes are distinguished; for molecular species, the vibrational and rotational internal modes, whose distribution functions, at a first approximation, may be characterized respectively by a vibrational and rotational temperature, are described. The local chemical equilibrium composition of the gas is determined from the equilibrium constants of the chemical reactions at the local translational temperature; local thermal equilibrium is defined by the equality of the translational, electronic, vibrational and rotational temperatures.

When the vibrational relaxation time τ_{vib} (which represents the characteristic time needed for a species with a given vibrational distribution function to regain its equilibrium vibrational distribution function) is comparable with the flow characteristic time τ_{flow}, the gas is out of thermal equilibrium. If τ_{vib} is much larger than τ_{flow}, the gas is said to be vibrationally frozen. When the characteristic time for a chemical reaction to reach equilibrium, τ_{chem}, is larger or comparable with τ_{flow}, the gas is out of chemical equilibrium.

For the main class of flows of interest here, the rotational relaxation time is much shorter than the flow characteristic time, so that the rotational and the translational temperature are equal. It is also assumed that vibrational relaxation processes are faster than chemical reactions; therefore, thermal equilibrium, when reached, is established before chemical equilibrium.

2.2. Governing equations

The set of conservation equations representing a non-equilibrium flow is composed of one conservation of mass equation per species, a vector momentum equation, and equations governing the total energy and the vibrational energy of each molecular species. The electron/electronic coupling with other internal modes is neglected, and electric neutrality of the gas is assumed when ionization occurs. This set of equations is detailed briefly below in a differential form (e.g. see [7,8]).

The conservation of mass for species i may be written in the form

$$\frac{\partial \rho_i}{\partial t} + \nabla\cdot(\rho_i \boldsymbol{u} + \boldsymbol{w}_{\text{d}i}) = \Omega_{\text{c}i} \tag{1}$$

where ρ_i is the density of species i, $\boldsymbol{u}$ is the mass average velocity, and $\boldsymbol{w}_{\text{d}i}$ is the diffusion velocity of species i. The diffusion velocity is modeled by Fick's law, neglecting the thermal gradient and pressure gradient terms, since these diffusion effects are weak for the application problems under study. The source term $\Omega_{\text{c}i}$ is the net rate of production of species i due to chemical reactions.

The momentum equation in vector form is

$$\frac{\partial \rho \boldsymbol{u}}{\partial t} + \nabla\cdot(\rho \boldsymbol{u}\boldsymbol{u}) + \nabla p = \nabla\cdot\tau \tag{2}$$

where p is the pressure of the gas based on Dalton's law, and τ denotes the stress tensor given by the classical constitutive relation for Newtonian fluids.

Conservation of total energy E is described by

$$\frac{\partial E}{\partial t} + \nabla\cdot(\boldsymbol{u}(E+p)) = \nabla\cdot(\tau:\ \boldsymbol{u}) - \nabla\cdot(q_{\text{t}} + q_{\text{v}}) + \sum_i \nabla\cdot(\rho_i h_i(\boldsymbol{u} - \boldsymbol{w}_i) + Q_{\text{rad}}) \tag{3}$$

where q_{t} is the translational heat flux, q_{v} is the vibrational heat flux, Q_{rad} is the radiative heat transfer, and h_i is the enthalpy of the species i per unit mass.

Finally, the vibrational energy of each molecular species is governed by

$$\frac{\partial E_{vj}}{\partial t} + \nabla\cdot(\boldsymbol{w}_j E_{vj}) = -\nabla\cdot q_v + \Omega_{vj} \tag{4}$$

where E_{vj} is the vibrational energy of species j, and Ω_{vj} is the vibrational source term due to thermal and chemical non-equilibrium.

The heat fluxes are assumed to satisfy a Fourier law

$$q_t = -k\nabla T, \qquad q_{vj} = -k_{vj}\nabla T_{vj} \tag{5}$$

where T is the translational temperature, T_{vj} is the vibrational temperature of the molecular species j, and k, k_v are the translational and vibrational thermal conductivities respectively. The equations for the transport properties (Schmidt number, viscosity and conductivity) are given in Appendix A.

2.3. Non-equilibrium source terms

The net rate of production of species i is obtained from chemical kinetic theory (see [7,9]). For a reaction involving species A_i, we have

$$\sum_i \alpha_i A_i \overset{k_f}{\underset{k_b}{\leftrightarrow}} \sum_j \beta_j A_j \tag{6}$$

It is assumed that the reaction set comprises a reaction mechanism, i.e. the set of reactions represents the processes actually occurring at the molecular level. Then, the net rate of production of species A_i is formally given by

$$\frac{\mathrm{d}}{\mathrm{d}t}[A_i] = (\beta_i - \alpha_i)\left(k_b \prod_j [A_j]^{\beta_j} - k_f \prod_j [A_j]^{\alpha_j}\right) \tag{7}$$

where α_i and β_i are the stoichiometric coefficients in the reactant or product A_i of reaction (6), $[A_i]$ is the concentration of species A_i, and the forward and backward rate coefficients are k_f and k_b respectively.

The source term Ω_{ci} is then the product of the molar mass of the species $[A_i]$ times the sum over all chemical reactions of the net rates of production of the species $[A_i]$. For a gas in thermal equilibrium at temperature T, the kinetic rate coefficients may be related by

$$\frac{k_{f,eq}}{k_{b,eq}} = K_e(T) \tag{8}$$

The forward equilibrium rate coefficient is assumed to satisfy the Arrhenius law detailed in Appendix A. The next section presents a discussion of the non-equilibrium rate coefficients.

Numerous curve-fits have been published for reactions that model the kinetics of nitrogen or air at high temperatures [10,11]. The equilibrium constant curve-fit formulas published by various authors are generally in good agreement, except at low translational temperature ($T \leq 1000$ K), or very high temperatures ($T \geq 15000$ K). However, the rate coefficients are not predicted as precisely as the equilibrium constants and order of magnitude differences may be noted between two different formulas describing the same rate coefficient [10–12]. Therefore, the non-equilibrium rate coefficients are also predicted within a certain error, since they are proportional to the equilibrium rate coefficients, as discussed in Subsection 2.4.

2.4. Non-equilibrium rate coefficients

When the gas is out of thermal equilibrium, the rate coefficients should be corrected to take into account the vibrational and rotational distribution of the molecules acting in a chemical reaction [13].

We present a new theoretical model of the non-equilibrium rate coefficients considering the effect of the vibrational distribution of all molecular species involved in a given chemical reaction. This theoretical correction may be expressed as

$$k_f = F(T, \{f_{vj}\})k_{f,eq}(T), \qquad k_b = G(T, \{f_{vj}\})k_{b,eq}(T) \tag{9}$$

where $\{f_{vj}\}$ is the vibrational distribution function of the molecular species j, which participates in reaction (6) as a reactant or product. Expressions for F and G are derived in Appendix A.

From Equations (9), we obtain

$$\frac{k_f}{k_b} = V(T, \{f_{vj}\})K_e(T) \tag{10}$$

At equilibrium, when the set $\{f_{vj}\}$ are described by Boltzmann distributions, each defined by the unique translational temperature, V is equal to 1. Equation (10) contradicts the common implicit assumption that V equals 1 for thermal non-equilibrium [7,13–15]. This assumption was discussed by Widom [16], who emphasized that the ratio of k_f/k_b, where k_f and k_b are obtained from experimental data, is indeed not equal to the equilibrium constant.

The calculation of F, G and V requires knowledge of state-to-state rate coefficients. Since these rates are not yet available in the literature for the reactions of interest here, the relations above are of limited practical use and remain theoretical, though they underline the need for additional work in this area. Hence, further simplifying assumptions are needed to carry on the modeling of the kinetics of chemical reactions.

Numerous models have been published in the literature to give a correction function F for the forward rate coefficient [17–19]. These models are founded on two assumptions: (1) the molecular species is a harmonic oscillator, and (2) its vibrational distribution function is described by a Boltzmann distribution. Treanor and Marrone [18] derived a correction function F based on the assumption of a Boltzmann distribution of harmonic oscillators. They also assumed that a molecular species i in a vibrational state v dissociates with a probability P_v, which follows an exponential law:

$$P_v = \exp\left(-\frac{T_{di} - \epsilon_{vi}/R_g}{U} \right) \tag{11}$$

where T_{di} is the dissociation temperature of the molecular species i, ϵ_{vi} is the energy of the vibrational level v, and U is a parameter equivalent to a pseudo-temperature that determines the extent of bias towards dissociation from excited vibrational states.

We note that for a dissociation/recombination reaction such as

$$\mathrm{N_2 + M} \overset{k_f}{\underset{k_b}{\leftrightarrow}} \mathrm{N + N + M} \tag{12}$$

Equation (11) is independent of the colliding partner M. If M is a molecule, it is implicitly assumed that its vibrational state is not modified by collision with N_2. Then the rate coefficients do not depend on the vibrational distribution of the colliding partner M. The correction function derived in [18] is

$$F_1 = \frac{Q(T_a)Q(T)}{Q(T_v)Q(-U)} \tag{13}$$

where

$$\frac{1}{T_a} = \frac{1}{T_v} - \frac{1}{T} - \frac{1}{U}$$

and Q is the vibrational partition function of species i. For U infinite, we recover the non-preferential dissociation model [17,18] for which the function correcting the forward rate is

$$F_2 = \frac{\Theta_{vi}}{T} \frac{\left(\exp\left(\frac{\Theta_{vi}}{T_v} \right) - 1 \right)\left(1 - \exp\left(\frac{-T_{di}}{T_a} \right) \right)}{\left(\exp\left(\frac{\Theta_{vi}}{T_a} \right) - 1 \right)\left(\exp\left(\frac{\Theta_{vi}}{T} \right) - 1 \right)} \tag{14}$$

where Θ_{vi} is the characteristic vibrational temperature of species i. Knab *et al.* [19] derived the coupled vibration chemistry vibration (CVCV) model also assuming that the rate coefficient is independent of the vibrational distribution of M. These correction functions F_1 and F_2 may be derived from the general form of the correction function given in Equation (9) (see Appendix A).

2.5. Vibrational source term

The vibrational source term due to chemical and thermal non-equilibrium is modeled as

$$\Omega_{vj} = \Omega_{v_1 j} + \Omega_{v_2 j} = \frac{E^*_{vj} - E_{vj}}{\tau_j} + \Omega_{cj} \frac{E_{vj}}{\rho_j} \tag{15}$$

where E^*_{vj} corresponds to the vibrational energy of species j if it were in thermal equilibrium at local translational temperature T, τ_j is the vibrational relaxation time of species j determined by a mole fraction weighted average over collision partners, which are the gas species,

$$\frac{1}{\tau_j} = \sum_i \frac{\chi_i}{\tau_{ij}} \tag{16}$$

with χ_i as the mole fraction of species i, τ_{ij} for species j is obtained from the Millikan and White curve-fit formula [20] and experimental laws given by Thivet *et al.* [21] for the molecule–atom vibrational–translational (V–T) relaxation times. The Millikan and White curve-fit formulae are inappropriate for molecule–atom interactions since they overpredict the V–T relaxation time for molecule–atom interaction by several orders of magnitude (see Appendix A).

The first term, $\Omega_{v_1 j}$, in (15) represents the rate of change of vibrational energy due to the net rate of change of the population of each vibrational level [15]. The second term, $\Omega_{v_2 j}$, takes into account the rate of change of vibrational energy induced by dissociation or recombination of the species j [18,19,22]; e.g. Treanor and Marrone [17] suggested an expression of $\Omega_{v_2 j}$ in the form

$$\Omega_{v_2 j} = \Omega_{cdj} E_{dj} + \Omega_{crj} E_{rj} \tag{17}$$

where Ω_{cdj} is the rate of destruction of the molecule j, Ω_{crj} is the rate of creation of molecule j, E_{dj} is the average vibrational energy lost by disintegration of molecule j, and E_{rj} is the average vibrational energy gained by recombination processes of molecule j. This more complex model accounts for the different energies released during dissociation and recombination processes, with E_d and E_r based on the assumptions of harmonic oscillators and Boltzmann distribution of the vibrational states. Here, we consider the simplified approach of non-preferential dissociation, which gives $E_{dj} = E_{rj} = E_{vj}$. The vibration–vibration (V–V) coupling is considered in Reference [21] and the vibration–electron (V–e) coupling in Reference [23]. In the present work, only the V–T coupling is retained, for simplicity, since the physical models associated with V–V and V–e coupling are still in question.

3. RADIATIVE NON-EQUILIBRIUM VISCOUS FLOW IN A PLASMA TORCH

3.1. Radiative model

The investigation here of radiative transfer is specifically directed to the plasma torch problem, and a simple layer model is introduced for preliminary studies of non-equilibrium flow in a plasma torch. Subsection 3.2 presents the plasma torch problem, and computational results are discussed.

It is assumed that the center of the jet is at high translational temperature ($T \geq 7000$ K) as a first step towards a more detailed treatment; the translational temperature decays with a strong radial gradient to low values ($T \leq 500$ K) outside the jet. We further assume that the

temperature is nearly constant in the cold region of the flow. Assuming that a local point in the gas, in the center of the jet, behaves as a black body emitting in a vacuum, then the shortest wavelength at which there is significant emission at $T = 7000$ K is $\lambda = 412$ nm. From the curve-fit, the absorption coefficient at pressures less than 10 atm is less than $10^{-2}\,\mathrm{cm}^{-1}$. Since the diameter of the jet is less than 1 cm, the gas is locally optically thin in the center of the jet. Similar reasoning indicates that the gas is locally optically thick in the cold region of the test chamber. We use the diffusion approximation to evaluate the radiative flux in an optically thick gas

$$q_r = -\frac{16\sigma T^3}{3a_{\mathrm{R}}}\nabla T \tag{18}$$

where σ is the Stefan–Boltzman constant and a_{R} is the Rosseland absorption coefficient [24]. This approximation is valid only for small temperature gradients. The diffusion approximation also fails close to a black boundary.

If we consider only emission, the radiative transfer for an optically thin gas is also given by a simple relation

$$Q_{\mathrm{rad}} = a\sigma T^4 \tag{19}$$

where a is the absorptivity of the gas.

The radiative transfer in the optically thick zone is defined by

$$Q_{\mathrm{rad}} = \nabla \cdot q_r \tag{20}$$

with q_r given by Equation (18). This model fails at the interface of the two regions and at the wall boundary. We further assume that the absorption coefficient varies with the temperature according to the following curve-fits obtained from Reference [25]: at $p = 1$ atm, if $T < 7000$ K, $a = 10^{3.78}$, if $T > 7000$ K then $a = 10^{-2.2} + (10^{-3.7} - 10^{-2.2})[(T - 12000)/5000]$. The corrections to the absorption coefficient due to non-equilibrium are neglected. Between the two layers, a 'buffer layer' is assumed, in which the absorption coefficient varies with temperature. The diffusion approximation is also used in this buffer zone. The resulting simple model provides a straightforward method to couple the radiative transfer calculation with the flow field calculation, when the flow field is divisible approximately into optically thick and thin regions. This model is applied in the following example.

3.2. Plasma torch problem

The results discussed here are for a plasma torch test problem, which was proposed in the *First Workshop on Hypersonic Flows for Reentry Problems* [2]. The present calculations were made with two objectives in mind. First, we wished to test the physical model presented above and implemented in the numerical scheme discussed in Part II, by comparing the results with those of Reference [23], where the same problem is solved by a different numerical scheme. (The comparison with another numerical simulation is needed because of the large uncertainties

associated with the modeling of reaction and relaxation rates.) Second, we wanted to compare the numerical results with experimental data available for this problem. In the torch problem, the nitrogen plasma enters through a constrictor of radius 3 mm, and expands in a test chamber of radius 10 cm (Figure 1). The translational temperature at the wall is fixed at 300 K; the normal gradient of the vibrational temperature is set equal to zero at the wall. The wall is also assumed to be non-catalytic. The pressure at the exit of the domain is fixed at 250 torr (about 33.3 kPa). The inlet profiles considered here are those proposed in [23] (modified profiles from [2]). We chose these inlet profiles in order to compare the present results with numerical results from [23]. Calculations of the Navier–Stokes equations in a constrictor of radius 3 mm show that the profiles remained almost constant with the axial position (Figure 2). The mesh for the torch was structured (120×80 nodes), with clustering near the axis of symmetry, and near the inlet plane. Iterations were carried out until the residual for the system was reduced below a tolerance of 10^{-3}. The explicit scheme required 3600 iterations to reach

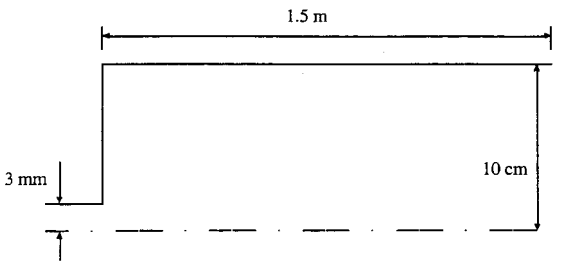

Figure 1. Plasma torch geometry (not to scale).

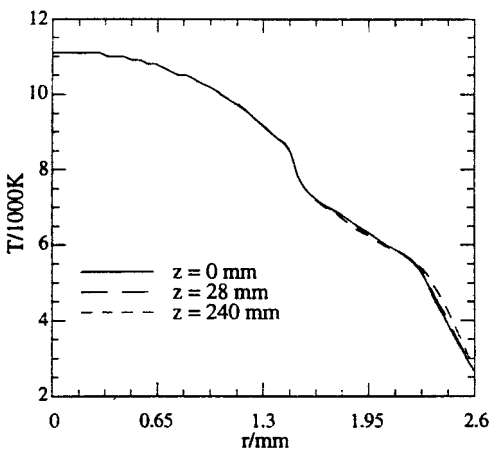

Figure 2. Profiles of translational temperature at three different axial locations in a duct of radius 3 mm.

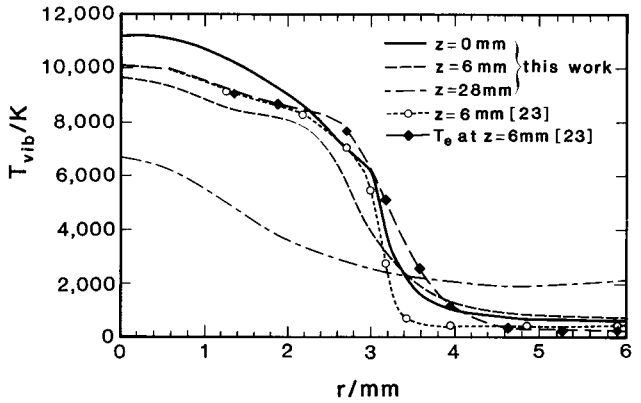

Figure 3. Computed radial profiles of vibrational temperature at three locations. The computed vibrational and electronic temperature profiles at $z = 6$ mm from Reference [23] are shown for comparison.

this residual. The implicit version of the code required 450 iterations at a maximum Courant–Friedrich–Lewy (CFL) number of 5.

Figures 3 and 4 show that the vibrational and translational temperatures decrease rapidly with increasing radius around the axis of symmetry. The vibrational temperature freezes at around $r = 3.5$ mm, and the translational temperature decays from 1000 K at the edge of the jet to the wall temperature. At a given axial location in the jet section, both the computed translational and vibrational temperatures are lower than those given in [23]. The maximum difference in the translational temperature is 200 K, while the difference is as large as 1000 K

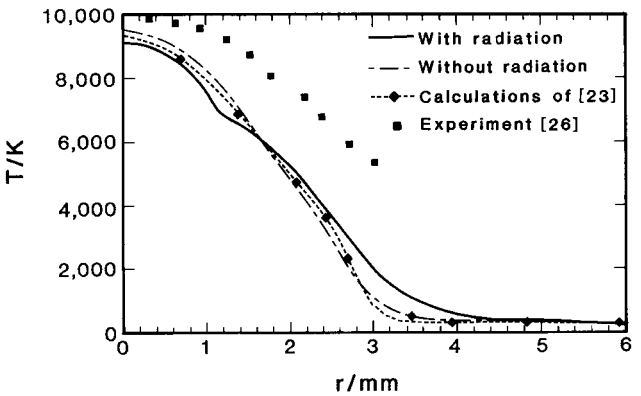

Figure 4. Translational temperature profile at $z = 6$ mm computed with and without effects of radiation. The calculated profile from Reference [23] and the experimental data from Reference [26] at the same axial location are also shown.

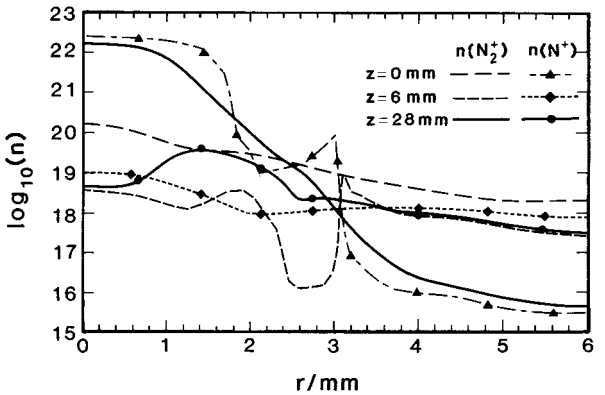

Figure 5. Computed electron and nitrogen atom number density profiles at three axial locations. The experimental data from Reference [26] at $z = 6$ mm are also shown for comparison.

for the vibrational temperature (see Figure 3). The difference arises partly because of the difference in the numerical scheme and partly because Rostand used a three-temperature model (translational, vibrational and electron/electronic temperatures). The species density profiles at different axial locations in Figures 5 and 6 show the variation in the solution behavior along the axis of symmetry. At the inlet plane ($z = 0$ mm), the number density profiles are discontinuous at the edge of the torch ($r = 3$ mm), where the incoming jet boundary (with Dirichlet conditions) and the wall boundary meet. The computed solution is not fully converged in this region. Note that the species density plots are given on a logarithmic scale, which tends to exaggerate the magnitude of small oscillations.

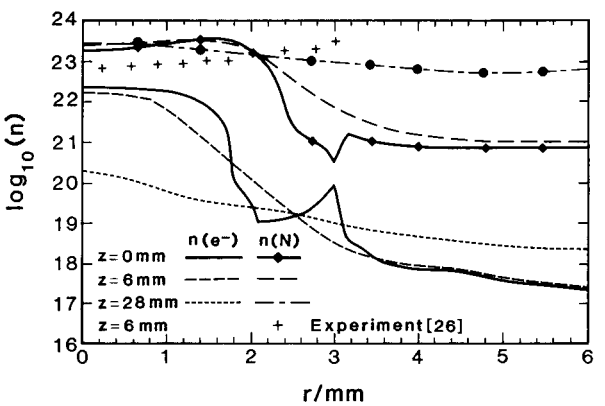

Figure 6. Computed nitrogen molecular ion (N_2^+) and atomic ion (N^+) number density profiles at three axial locations.

The experimental data at the inlet plane were only specified for $r < 2.3$ mm and were extrapolated to $r = 3$ mm. As noted above, these profiles correspond to nearly fully developed flow and hence appear reasonable. The discontinuities in e^-, N^+ and N profiles are a relatively small fraction ($\simeq 1$ per cent) of the peak values. Although the discontinuity in the N_2^+ profile at $z = 0$ in Figure 6 is very large relative to its absolute value in the core region, it is a minor species with density about three orders of magnitude smaller than e^- or N^+. The discontinuities in these quantities near the corner, coupled with the requirement of strict charge neutrality, lead to the large discontinuity in the density profile of N_2^+. The number density profiles, like the temperature profiles, also show strong gradients in the radial direction around the edge of the jet. Further downstream, the number densities decay very slowly, or reach a constant value, where the vibrational temperature freezes. The results at the edge of the jet are probably affected by the inlet plane profiles. The number densities of electrons and N^+ decrease with increasing axial co-ordinate around the axis of symmetry, while they remain nearly constant outside the jet. The decrease of N^+ and electrons near the centerline results from the formation of N atoms by recombination of these species. Dissociation of N_2 also contributes to the increase in N atom density near the centerline (see Figure 5). The ionized species reach a frozen number density outside the jet, where the vibrational temperature freezes. However, the number density of N atoms does not reach a constant value. This is because the translational temperature at the edge of the jet is still about 1000 K, and dissociation of N_2 is still significant. The density profiles obtained in these calculations are in good agreement with those of Reference [23]. This is also true of the electron density profiles even though our model does not have a separate electron temperature. This may be due to the fact that we assumed $T_e = T_v$.

The effect of the radiative model is shown in Figure 4. The temperature profile has a discontinuous gradient at $T = 7000$ K. This corresponds to the crude approximation that the gas is optically thin for $T > 7000$ K, and optically thick for $T < 7000$ K. The radiative calculation shows that at a given radial location in the optically thin region, the temperature is 300–500 K less than the computed temperature, with radiation effects omitted. For an optically thin gas, the absorption is negligible relative to emission. Thus, the gas is cooled, whereas the reverse occurs for an optically thick gas. These trends are observed in Figure 4. The difference in temperature prediction is not negligible, indicating more complex radiative calculations may be needed.

Experimental data from Reference [26] are also shown where available. Figure 5 shows that the model predictions are within a factor of two for the number densities. The translational temperature profiles in Figure 4 are also in good agreement except near the centerline, where they differ by less than 1000 K ($\simeq 10$ per cent). Large gradients are observed on the edge of the jet, where the experimental data decay at a slower rate. This may be due to turbulence in the edge of the jet. The calculations performed in this test problem demonstrate the capability of the numerical code to handle viscous non-equilibrium flow in a test chamber. The comparison of the numerical results with experimental data is not fully satisfactory, and will be the subject of continuing investigation.

4. NON-EQUILIBRIUM FLOW IN A CONVERGING–DIVERGING NOZZLE

This test problem was proposed in Reference [27]. The converging section of the nozzle is defined by an arc of a circle of radius 1.47 cm. The diverging section is a cone of half angle 10°, 1.03 m long. The radius at the throat is 3 mm. The throat is defined by a circular arc of radius 2 cm, connected to the converging section at 45°, and to the diverging cone at 10°. The radius at the exit plane is 20 cm. The total length of the converging diverging nozzle is 1.08 m.

The goal is to compare inviscid non-equilibrium calculations in an axisymmetric nozzle with reference solutions in the literature. Two different models are also compared to describe the kinetic rate coefficients, and to carry out related sensitivity studies using results for non-equilibrium rate coefficients of N_2 diluted in Ar provided by Gonzales [13].

Using the numerical scheme detailed in Part II, the solution is computed on a 180×25 structured grid, which is highly clustered in the throat region (33 per cent of the nodes are located in a zone delimited by the inlet plane, and a plane at $x = 0.1$ m from the inlet). The stagnation pressure is 1530 MPa, and the stagnation temperature is 6500 K. The inlet flow is assumed to be in chemical equilibrium and a slip condition is enforced at the wall of the nozzle. The initial solution is chosen as the quasi one-dimensional solution for a perfect gas, assuming that the gas mixture is in chemical equilibrium. The solutions were taken to be converged at a residual of 10^{-4}.

The set of chemical reactions is the same as in References [22,28] but the models for the kinetic rate coefficients and the vibrational energy equations differ from the current ones. Both [22] and [28] used distinct vibrational temperatures to describe the vibrational distributions of N_2 and O_2, and assumed that the vibrational distribution of NO is described by the translational temperature. In the present work, only one vibrational temperature, T_{v,N_2}, is used to characterize the vibrational distribution of all the molecular species, whereas [22] used Equation (17) to model the vibrational source term. Figures 7 and 8 compare the mass fraction of NO and O_2 respectively along the axis of symmetry in the diverging section. All solutions indicate that the species mass fractions freeze very close to the throat in the diverging section.

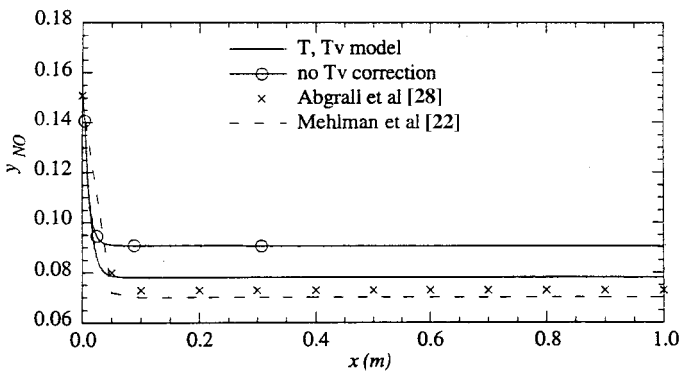

Figure 7. NO mass fraction comparison along the axis of symmetry of a diverging nozzle.

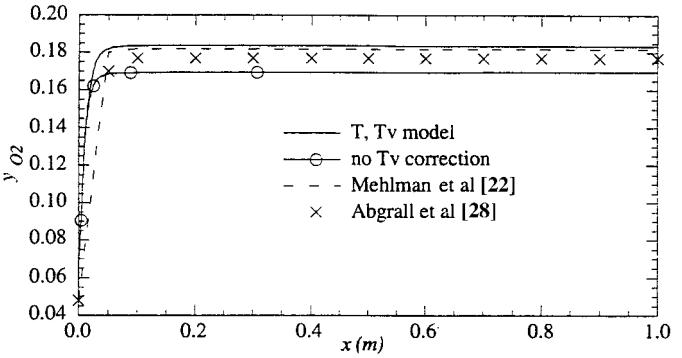

Figure 8. O_2 mass fraction comparison along the axis of symmetry of a diverging nozzle.

We note that for a mixture coresponding to the frozen flow at $T = 3000$ K (i.e. $y_{N_2} = 0.74$, $y_{O_2} = 0.19$, $y_{NO} = 5.64 \times 10^{-2}$, $y_N = 0.0$, $y_O = 4.0 \times 10^{-3}$, with y denoting the mass fraction), then the ratio of the vibrational relaxation times of the molecular species are: $\tau_{N_2}/\tau_{O_2} = 100$, and $\tau_{N_2}/\tau_{NO} = 25$, which implies that the molecular species O_2 and NO relax faster than N_2.

The results from the present work indicate that NO and O_2 concentrations freeze at the same location $x = 0.05$ m. The results from [22,28] show that the mass fractions of NO and O_2 freeze further downstream than predicted in the current calculations. In the current calculations, τ_{v,N_2} freezes at 4150 K versus 2050 K in [28]. Consequently, the vibrational temperature freezes closer to the throat in the current work than in the results provided by [27]. We emphasize that our model for the vibrational energy equation is different from [22]. Figure 8 shows that the mass fraction at which oxygen freezes is different in each study. This difference is attributed to the use of different models for the rate coefficients. Two models of the rate coefficients were used in our calculation. The first model assumed the rate coefficient to be unaffected by thermal non-equilibrium; a second model corrected the rate coefficients using Equation (37) (see Appendix A) and is labeled as the 'T, T_v model' in the figures. The calculations indicate a 10 per cent difference between the freezing mass fractions of both NO and O_2 for the two models. At $T = 3000$ K, $T_v = 4000$ K (values at $x = 0.05$ m Figure 8), the rate coefficient of the dissociation/recombination reaction $O_2 \leftrightarrow O + O$, corrected for non-equilibrium using (37), is a thousand times larger than the rate coefficient at thermal equilibrium. In the expansion region, the net reaction is recombination of O atoms to form O_2, and thus the two-temperature model that predicts higher reaction rates predicts higher O_2 levels than the single-temperature model.

We note that the net rate of production of NO due to the dissociation/recombination reaction $NO \leftrightarrow N + O$, is orders of magnitude lower than that due to the reactions $NO + O \leftrightarrow N + O_2$ and $N_2 + O \leftrightarrow N + NO$ (denoted by R_1 and R_2 respectively). At $T = 3000$ K, R_1 depletes N and O_2, at a rate $\omega_1 = k_{b,R_1}[O_2][N]$, while R_2 depletes NO and N at a rate $\omega_2 = k_{b,R_2}[NO][N]$. Let $\omega_2/\omega_1 = \theta$. At $x = 0.05$ m, $T = 3000$ K and $T_v = 4000$ K, the ratio θ (T, T_v model)/θ (no correction) is of order 1000. This indicates that more depletion of NO occurs when the 'T, T_v model' is used. This explains the observation that the frozen mass

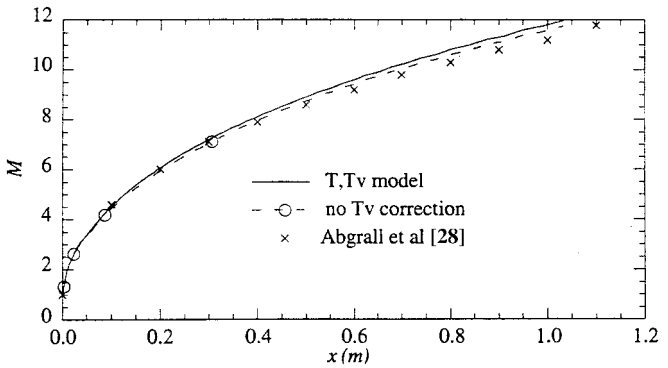

Figure 9. Mach number comparison along the axis of symmetry of a diverging nozzle.

fraction of NO for the 'T, T_v model' using Figure 7 is less than that obtained without correction, whereas y_{O_2} ('T, T_v model') is larger than y_{O_2} ('no correction') (Figure 8). The influence of the rate models on the overall gas properties is not negligible. Figure 9 shows a comparison of the Mach number on the axis of symmetry, for the present calculations and the results given in [28]. The exit Mach number obtained with the 'T, T_v model' differs from the value obtained in [28] by 5 per cent. We also note that our calculations show a difference of 2.5 per cent for the exit Mach number computed with the two rate coefficients models. Figure 10 compares the translational temperature on the axis of symmetry. It shows that the exit temperature differs from the value obtained in [28] by 30 K. This figure also indicates the sensitivity of the translational temperature to the model for the rate coefficients. Two calculations were made, one using the 'T, T_v model' and the other with all rates ten times larger. The exit temperature for these two cases differs by 50 K. This difference is relatively small compared with the stagnation temperature (6500 K), yet significant relative to the exit

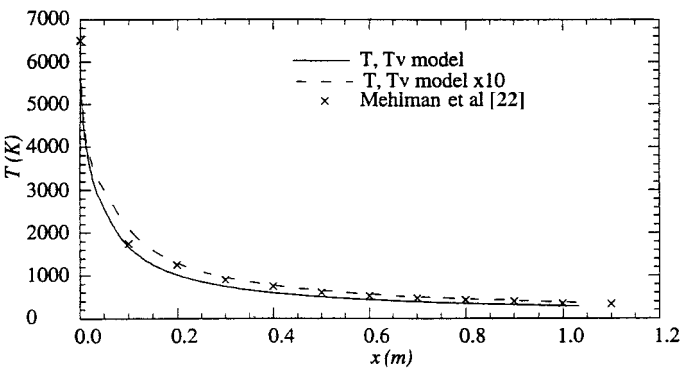

Figure 10. Translation temperature comparison along the axis of symmetry of a diverging nozzle.

temperature from the 'T, T_v model' (312 K). For this test case, good agreement has been obtained in the calculations of the bulk flow properties for a non-equilibrium calculation in a diverging nozzle. However, this test case clearly indicates that the flow composition depends significantly on the models for the rate coefficients.

5. CONCLUDING REMARKS

In Part I, a class of physical models has been extended to describe a multi-species reacting gas, and an alternate relation for the chemical reaction rate coefficients has been determined. It should be noted that while the physical model used for flow field calculations is standard, many issues concerning non-equilibrium kinetic rate coefficients, vibrational distribution functions of molecular species, and absorption coefficients, remain the subject of current research. In Part II, we describe the hybrid finite element/finite volume scheme used to compute the approximate solutions for this model. We anticipate that this simulation capability will permit us to explore general trends and in some instances provide detailed results. The simulation may also provide a 'platform' for improved models as they are developed.

APPENDIX A

A.1. Transport properties

Several formulas and curve-fits are needed to compute kinematic viscosity, thermal conductivity, and Schmidt number for species N_2, O_2, NO, N, O, N_2^+, N^+, and e^-. For perfect gas calculations, it is assumed that all the species are the same. The viscosity of the gas is obtained by Sutherland's law

$$\mu(T) = \mu(T_{\text{ref}})\left(\frac{T}{T_{\text{ref}}}\right)^{1.5}\left(\frac{T_{\text{ref}}+110}{T+110}\right) \tag{21}$$

At $T_{\text{ref}} = 300$ K, μ (300 K) $= 1.81 \times 10^{-5}$ kg m^{-1} s^{-1}.

We assume $Pr = 0.72$, then the thermal conductivity is

$$k(T) = \frac{\mu(T)c_p}{Pr}, \quad c_p = \frac{\gamma}{\gamma - 1}\frac{R_g}{M} \tag{22}$$

For a multi-species gas, each species has its own transport properties.

The viscosity of each species is determined by Blottner's curve-fit

$$\mu_i = 0.1 \exp((a \ln(T) + b)\ln(T) + c) \text{ kg m}^{-1}\text{ s}^{-1} \tag{23}$$

where (a, b, c) for N_2, O_2, NO, N and O are respectively

$$(0.02681, 0.31778, -11.3155), (0.044929, 0.082616, -9.20195), (0.043638, 0.033551, -9.57674), (0.020314, 0.42944, -11.60314), (0.01156, 0.60317, -12.43275)$$

$\mu(N_2^+) = \mu(N_2)$; $\mu(N^+) = \mu(N) \times 13.3^{\alpha}$, with $\alpha = (\rho_N^+ + \rho_N)/\rho$ being the degree of ionization.

The mixture viscosity is obtained from Wilke's law

$$\mu = \sum_i \frac{\mu_i \chi_i}{\sum_j \chi_j \left(1 + \left(\frac{\mu_i}{\mu_j}\right)^{1/2} \left(\frac{M_j}{M_i}\right)^{1/4}\right)^2 \left(8\left(1 + \frac{M_j}{M_i}\right)\right)^{1/2}} \tag{24}$$

The thermal conductivity of each atom species is obtained from the viscosity by the relation $k_i = (15/4)(R_g/M_i)\mu$ and Eucken's relation $k_i = [c_p + (5/4)(R_g/M_i)]\mu$ for diatomic molecules.

The thermal conductivity of a mixture is also obtained by Wilke's law. The vibrational conductivity of species i is obtained from the relation

$$k_{vi} = \mu_i \frac{\partial E_{vi}/\rho_i}{\partial T_{vi}} \tag{25}$$

The Schmidt number is taken to be 1 for neutral species, and 2 for ionized species.

The relaxation time of a species i in a gas mixture is given by the relation [7]

$$\tau_i = \tau_{MW_i} + \tau_{C_i} \tag{26}$$

where $\tau_{MW_i} = \Sigma_j \chi_j/\tau_{ij}$ and $\tau_{C_i} = 1/\chi_i \sigma N_i$, $\chi_i = \sqrt{8R_gT/\pi M_i}$, $\sigma = 10^{-21} \times (50000/T)^2$ m^2. Here N_i is the number density of species i, χ_j is the mole fraction of species j, and τ_{ij} is given by the relation due to Millikan and White [20]

$$p\tau_{ij} = \exp(A_{ij}(T^{-1/3} - 0.015\mu_{ij}^{1/4}) - 18.42) \tag{27}$$

$$A_{ij} = 1.16 \times 10^{-3} \mu_{ij}^{1/2} \Theta_{vi}^{4/3} \tag{28}$$

$$\mu_{ij} = \frac{M_i M_j}{M_i + M_j} \tag{29}$$

where Θ_{vi} is the characteristic vibrational temperature of species i, p is the pressure of the gas in atmospheres, the reduced masses are in atomic mass units (and τ_{ij} are extrapolated for temperatures higher than 6000 K).

A.2. Equilibrium constants, equilibrium rate coefficients

The curve-fits for equilibrium constants have the form

$$K_e = \exp(A_1/z + A_2 + A_3 \ln z + A_4 z + A_5 z^2) \tag{30}$$

with $z = 10000/T$, and the constant coefficients given in [7] for a total number density of 10^{17}. The forward equilibrium rate coefficients were taken from [11], except for the reactions involving the species N^2, N_2^+, N, N^+, and e^- for which the rate coefficients were those used by [22]. The rate coefficients are assumed to satisfy an Arrhenius-type law

$$k_f = CT^s \exp\left(-\frac{T_d}{T}\right) \tag{31}$$

The values of the coefficients A_1–A_5, C, s, and T_d are given in Table I in MKS units. C is in $\mathrm{mol}^{-2}\,\mathrm{m}^6\,\mathrm{kg}^{-1}\,\mathrm{s}^{-1}$.

A.3. Non-equilibrium rate coefficients

We present here a derivation of the rate coefficients for a chemical reaction of the type

$$\mathrm{AB} + \mathrm{M} \leftrightarrow \mathrm{A} + \mathrm{B} + \mathrm{M} \tag{32}$$

and discuss the derivation of an expression for non-equilibrium rate coefficients given in [16]. Consider an elementary reaction $r(u, v, w)$ of the form

$$\mathrm{AB}(u) + \mathrm{M}(v) \underset{k^{\infty w}_{uv\mathrm{b}}}{\overset{k^{\infty w}_{uv\mathrm{f}}}{\leftrightarrow}} \mathrm{A} + \mathrm{B} + \mathrm{M}(w) \tag{33}$$

where $\mathrm{AB}(u)$ represents the molecule AB in the vibrational state u. The notation ∞ symbolizes the dissociation of the molecule AB. The net rate of production of AB is

$$\left.\frac{\mathrm{d}}{\mathrm{d}t}[\mathrm{AB}(u)]\right|_{r(u,v,w)} = k^{\infty w}_{uv\mathrm{b}}[\mathrm{A}][\mathrm{B}][\mathrm{M}(w)] - k^{\infty w}_{uv\mathrm{f}}[\mathrm{AB}(u)][\mathrm{M}(v)] \tag{34}$$

Since this relation is valid for all v and w,

$$\frac{\mathrm{d}}{\mathrm{d}t}[\mathrm{AB}(u)] = \sum_{v,w} \left.\frac{\mathrm{d}}{\mathrm{d}t}[\mathrm{AB}(u)]\right|_{r(u,v,w)} \tag{35}$$

As $[\mathrm{AB}] = \Sigma_u\,[\mathrm{AB}(u)]$, we have

$$\frac{\mathrm{d}}{\mathrm{d}t}[\mathrm{AB}] = \sum_u \frac{\mathrm{d}}{\mathrm{d}t}[\mathrm{AB}(u)] = \sum_u \sum_{v,w} k^{\infty w}_{uv\mathrm{b}}[\mathrm{M}(w)][\mathrm{A}][\mathrm{B}] - \sum_u \sum_{v,w} k^{\infty w}_{uv\mathrm{f}}[\mathrm{M}(v)][\mathrm{AB}(u)] \tag{36}$$

or

Table I. Equilibrium constants, rate coefficients.

Chemical reaction	Equilibrium constant					Forward rate coefficient		
	A_1	A_2	A_3	A_4	A_5	C	s	T_d/K
Dissociation/recombination reactions								
$N_2+N_2\leftrightarrow N+N+N_2$	1.535	15.41	1.299	−11.49	−0.006	7.0×10^{15}	−1.6	113 260
$N_2+O_2\leftrightarrow N+N+O_2$						3.7×10^{15}	−1.6	113 260
$N_2+NO\leftrightarrow N+N+NO$						3.7×10^{16}	−1.6	113 260
$N_2+N\leftrightarrow N+N+N$						3.0×10^{16}	−1.6	113 260
$N_2+O\leftrightarrow N+N+O$						1.1×10^{15}	−1.6	113 260
$N_2+e^-\leftrightarrow N+N+e^-$						1.1×10^{18}	−1.6	113 260
$O_2+N_2\leftrightarrow O+O+N_2$	0.554	16.27	1.776	−6.57	−0.031	2.75×10^{13}	−1.0	59 500
$O_2+O_2\leftrightarrow O+O+O_2$						2.75×10^{13}	−1.0	59 500
$O_2+NO\leftrightarrow O+O+NO$						2.75×10^{13}	−1.0	59 500
$O_2+N\leftrightarrow O+O+N$						8.25×10^{13}	−1.0	59 500
$O_2+O\leftrightarrow O+O+O$						8.25×10^{13}	−1.0	59 500
$NO+N_2\leftrightarrow N+O+N_2$	0.558	14.52	0.554	−7.530	−0.014	2.3×10^{11}	−0.5	75 500
$NO+O_2\leftrightarrow N+O+O_2$						2.3×10^{11}	−0.5	75 500
$NO+NO\leftrightarrow N+O+NO$						2.3×10^{11}	−0.5	75 500
$NO+N\leftrightarrow N+O+N$						4.6×10^{11}	−0.5	75 500
$NO+O\leftrightarrow N+O+O$						4.6×10^{11}	−0.5	75 500
Exchange reactions								
$N_2+N+\leftrightarrow N_2^++N$	0.045	−0.027	−1.478	−0.53	−0.04	2.00×10^{5}	0.81	13 000
$NO+O\leftrightarrow N+O_2$	0.0048	−1.744	−1.223	−0.96	−0.04	2.16×10^{5}	1.29	19 220
$O+N_2\leftrightarrow N+NO$	0.976	0.896	0.746	−3.96	−0.07	3.18×10^{10}	0.1	37 700
Ionization reactions								
$N+N\leftrightarrow N_2^++e^-$	−2.429	−5.047	−5.072	−5.697	−0.042	2.00×10^{7}	0	−67 500
$N+e^-\leftrightarrow N^++e^-+e^-$	0.932	−3.414	−2.295	−16.66	−0.0093	2.5×10^{27}	3.82	168 200

$$\frac{\mathrm{d}}{\mathrm{d}t}[\mathrm{AB}] = \sum_u \sum_{v,w} k_{uv\mathrm{b}}^{\infty w} \frac{[\mathrm{M}(w)]}{[\mathrm{M}]}[\mathrm{A}][\mathrm{B}][\mathrm{M}] - \sum_u \sum_{v,w} k_{uv\mathrm{f}}^{\infty w} \frac{[\mathrm{M}(v)]}{[\mathrm{M}]} \frac{[\mathrm{AB}(u)]}{[\mathrm{AB}]}[\mathrm{AB}][\mathrm{M}] \tag{37}$$

Setting

$$\sum_{u,v} k_{uv\mathrm{b}}^{\infty w} = k_{w\mathrm{b}} \tag{38}$$

$$\sum_w k_{w\mathrm{b}} \frac{[\mathrm{M}(w)]}{[\mathrm{M}]} = k_{\mathrm{b}} \tag{39}$$

and similarly

$$\sum_{v,w} k_{uv\mathrm{f}}^{\infty w} \frac{[\mathrm{M}(v)]}{[\mathrm{M}]} = \sum_v k_{uv\mathrm{f}} \frac{[\mathrm{M}(v)]}{[\mathrm{M}]} = k_{u\mathrm{f}} \tag{40}$$

and

$$\sum_u k_{u\mathrm{f}} \frac{[\mathrm{AB}(u)]}{[\mathrm{AB}]} = k_{\mathrm{f}} \tag{41}$$

Then, (37) becomes

$$\frac{\mathrm{d}}{\mathrm{d}t}[\mathrm{AB}] = k_{\mathrm{b}}[\mathrm{A}][\mathrm{B}][\mathrm{M}] - k_{\mathrm{f}}[\mathrm{AB}][\mathrm{M}] \tag{42}$$

Since $k_{uv\mathrm{b}}^{\infty w}$ and $k_{uv\mathrm{f}}^{\infty w}$ depend only on the translational temperature T, k_{b} depends on T and the vibrational distribution function of the colliding partner M; likewise, k_{f} depends on T and the vibrational distribution functions of M and AB. If M is an atom, a similar derivation, considering that M has no vibrational quantum states, gives a backward rate coefficient k_{b}, which depends only on T and a forward rate coefficient k_{f} that depends on T and the vibrational distribution function of AB.

Let us assume now that the vibrational states of all the molecular species are Boltzmann distributed but that the vibrational temperature is not necessarily the same as T. Then,

$$n_{\mathrm{M}(v)} = \frac{[\mathrm{M}(v)]}{[\mathrm{M}]} = \frac{\exp(-\epsilon_{v\mathrm{M}}/\kappa T_{\mathrm{vM}})}{Q_{\mathrm{vM}}(T_{\mathrm{vM}})} \tag{43}$$

where κ is the Boltzmann constant, $\epsilon_{v\mathrm{M}}$ is the energy at the quantum number v, and Q_{vM} the vibrational partition function. Then,

$$k_{\mathrm{b}} = \sum_v k_{v\mathrm{b}} \frac{\exp(-\epsilon_{v\mathrm{M}}/\kappa T_{\mathrm{vM}})}{Q_{\mathrm{vM}}(T_{\mathrm{vM}})} \tag{44}$$

and

$$k_{\mathrm{b,eq}} = \sum_v k_{v\mathrm{b}} \frac{\exp(-\epsilon_{v\mathrm{M}}/k_T)}{Q_{\mathrm{vM}}(T)} \tag{45}$$

So

$$k_{\mathrm{b}} = \frac{Q_{\mathrm{vM}}(T)}{Q_{\mathrm{vM}}(T_{\mathrm{vM}})} \frac{\sum_v k_{v\mathrm{b}} \exp(-\epsilon_{v\mathrm{M}}/k_{T_{\mathrm{vM}}})}{\sum_v k_{v\mathrm{b}} \exp(-\epsilon_{v\mathrm{M}}/k_T)} k_{\mathrm{b,eq}} \tag{46}$$

That is,

$$k_{\mathrm{b}} = G(T, T_{\mathrm{vM}}) k_{\mathrm{b,eq}} \tag{47}$$

Similarly, the forward rate coefficient can be rewritten as

$$k_{\mathrm{f}} = \sum_u k_{u\mathrm{f}} \frac{\exp(-\epsilon_{u\mathrm{AB}}/k_{T_{\mathrm{vAB}}})}{Q_{\mathrm{vAB}}(T_{\mathrm{vAB}})} \tag{48}$$

and

$$k_{u\mathrm{f}} = \sum_v k_{uv\mathrm{f}} \frac{\exp(-\epsilon_{v\mathrm{M}}/k_{T_{\mathrm{vM}}})}{Q_{\mathrm{vM}}(T_{\mathrm{vM}})} \tag{49}$$

so

$$k_{\mathrm{f}} = \frac{Q_{\mathrm{vM}}(T) Q_{\mathrm{vAB}}(T)}{Q_{\mathrm{vM}}(T_{\mathrm{vM}}) Q_{\mathrm{vAB}}(T_{\mathrm{vAB}})} \times \frac{\sum_u \sum_v k_{uv\mathrm{f}} \exp(-\epsilon_{v\mathrm{M}}/k_{T_{\mathrm{vM}}}) \exp(-\epsilon_{u\mathrm{AB}}/k_{T_{\mathrm{vAB}}})}{\sum_u \sum_v k_{uv\mathrm{f}} \exp(-\epsilon_{v\mathrm{M}}/k_T) \exp(-\epsilon_{u\mathrm{AB}}/k_T)} k_{\mathrm{f,eq}} \tag{50}$$

or

$$k_{\mathrm{f}} = F(T, T_{\mathrm{vM}}, T_{\mathrm{vAB}}) k_{\mathrm{f,eq}} \tag{51}$$

Furthermore, if we assume that $k_{uv\mathrm{f}}^{\infty w}$ is independent of v and w and neglect the vibrational states of the molecule M, the forward rate coefficient depends only on the translational temperature and the vibrational distribution function of AB.

Let us consider, for example, the reaction

$$\mathrm{NO} + \mathrm{N_2} \underset{k_{\mathrm{b}}}{\overset{k_{\mathrm{f}}}{\leftrightarrow}} \mathrm{N} + \mathrm{O} + \mathrm{N_2} \tag{52}$$

The correction function F depends on the translational temperature T and the vibrational distribution functions of both NO and N_2.

REFERENCES

1. Moss JN, Scott CD (eds). *Thermophysical Aspects of Re-entry Flow*. *Progress in Astronautics and Aeronautics*, vol. 103. AIAA: New York, 1986.
2. Desideri JA, Glowinski R, Periaux J. *Hypersonic Flows for Reentry Problems*, vols. I and II. Springer: Berlin, 1991.
3. Flament C, Coquel F, Marmignon C, Hollanders H. *Viscous nonequilibrium calculation by an implicit finite volume method*. AIAA Paper 91-0702, 29th Aerospace Sciences Meeting, Reno, NV, January 1991.
4. Candler G, McCormack RW. *The computation of hypersonic ionized flows in chemical and thermal non-equilibrium*. AIAA Paper 88-0511, 26th Aerospace Sciences Meeting, Reno, NV, January 1989.
5. Li CP. *Computing viscous reactive flow over blunt winged vehicles*. Proceeding of the 2nd Joint Europe/U.S. Short Course in Hypersonics, Colorado Springs, CO, January 1989.
6. Suresh A, Liou M. *The Osher scheme for real gases*. AIAA Paper 90-0397, 28th Aerospace Sciences Meeting, January 1990.
7. Park C. *Nonequilibrium Hypersonic Aerothermodynamics*. Wiley: New York, 1988.
8. Lee JH. Basic governing equations for the flight regime of aeroassisted orbital transfer vehicles. In Nelson HF (ed), *Progress in Astronautics and Aeronautics*, vol. 96. AIAA: New York, 1985; 3–53.
9. Williams F. *Combustion Theory*, 2nd edn. Benjamin–Cummings: Redwood City, CA, 1985.
10. Dunn MG, Kang SW. *Theoretical and experimental studies of reentry plasmas*. NASA CR 2232, April 1973.
11. Park C. *Convergence of computation of chemical reacting flows*. AIAA Paper 85-0247, January 1985; also in reference [1], p. 478.
12. Evans JS, Schexnayder CJ, Huber PW. *Boundary layer electron profiles for entry of a blunt slender body at high altitude*. NASA TN D-7337, July 1973.
13. Varghese PL, Gonzales DA. Non-equilibrium chemistry models for shock-heated gases. In Capitelli M (ed), *Molecular Physics and Hypersonic Flows*. NATO ASI Series. Kluwer: Dordrecht, 1996.
14. Anderson JD Jr. *Hypersonic and High Temperature Gasdynamics*. McGraw-Hill: New York, 1989.
15. Vincenti WG, Kruger CH. *Introduction to Physical Gas Dynamics*. Wiley: New York, 1965.
16. Widom B. Molecular transitions and chemical reaction rates. *Science* 1965; **148**: 1555–1560.
17. Treanor CE, Marrone PV. Effect of dissociation on the rate of vibrational relaxation. *Physics of Fluids* 1962; **5**: 1022–1026.
18. Marrone PV, Treanor CE. Chemical relaxation with preferential dissociation from excited vibrational levels. *Physics of Fluids* 1963; **6**: 1215–1221.
19. Knab O, Fruhauf HH, Jonas S. *Multiple temperature descriptions of reaction rate constants with regard to consistent chemical vibrational coupling*. AIAA Paper 92-2947, AIAA 27th Thermophysics Conference, Seattle, WA, July 1992.
20. Millikan RC, White DR. Systematics of vibrational relaxation. *Journal of Chemical Physics* 1963; **39**: 3209–3213.
21. Thivet F, Perrin MY, Candel S. A unified non-equilibrium model for hypersonic flows. *Physics of Fluids A* 1991; **3**: 2799–2812.
22. Mehlman G, Thivet F, Candel S, Dubois F. Computation of hypersonic flows with a fully coupled implicit solver and an extension of the CVDV model for thermochemical relaxation. Workshop on *Hypersonic Flows for Reentry Problems*, Part II, April 1991, Antibes (France), vol. 6, pp. 105–124, INRIA/GAMNI-SMAI.
23. Rostand P, McCormack RW. *CFD modeling of an arc heated jet*. AIAA 90-1475, AIAA 21st Fluid Dynamics, Plasma Dynamics, and Lasers Conference, Seattle, WA, June 1990.
24. Siegel R, Howell JR. *Thermal Radiation Heat Transfer*, 2nd edn. Hemisphere: New York, 1981.
25. Harlé C. *Navier–Stokes computations for non-equilibrium reacting gas flows*. PhD Thesis, Department of Aerospace Engineering, The University of Texas at Austin, August 1994.
26. Leger JM, Coudert JF, Grimaud A, Fauchais P. Study of a nitrogen DC plasma torch at different pressures using optical and thermal diagnostics. Workshop on *Hypersonic Flows for Reentry Problems*, Part I, January 1990, Antibes (France), vol. 6, pp. 3–30, INRIA/GAMNI-SMAI.
27. Desideri JA, Glowinski R, Periaux J (eds). *Hypersonic Flows for Reentry Problems*, vol. II. Springer: Berlin, 1991.
28. Abgrall R, Merlo A. Calculation of a hypersonic nozzle flow. Workshop on *Hypersonic Flows for Reentry Problems*, Part II, April 1991, Antibes (France), vol. 6, pp. 125–142, INRIA/GAMNI-SMAI.

